RSC Applied Polymers

ROYAL SOCIETY OF CHEMISTRY

PAPER

View Article Online
View Journal | View Issue

Cite this: *RSC Appl. Polym.*, 2024, **2**, 483

Ultrathin redox active hydrogel electrolytes for high performance flexible supercapacitors†

Mengmeng Xun,[a] Xiuting Shi,‡[a] Haiping Wang,[a] Xiaoyan Li,[a] Wenxing Miao,[a] Xiangbing Wang,[a] Kanjun Sun,[b] Hui Peng, [a] Guofu Ma *[a] and Yuxi Xu *[c]

Received 10th January 2024,
Accepted 6th March 2024

DOI: 10.1039/d4lp00007b

rsc.li/rscapplpolym

Flexible supercapacitors (FSCs) based on hydrogel electrolytes have the advantages of high ionic conductivity, no liquid leakage, flexibility and versatility, making them the most promising power sources for wearable devices. Herein, a flexible and stretchable, ultrathin polyvinyl alcohol/carboxymethyl chitosan incorporated with a redox active ionic liquid (PVA/CMCS-[ViEtIm][Br]) hydrogel electrolyte is prepared by a facile coating and freezing/thawing method, which is used to improve the practical performance of supercapacitors. The PVA/CMCS-[ViEtIm][Br] hydrogel film has good mechanical properties. More importantly, the redox reaction caused by [ViEtIm][Br] in the hydrogel electrolyte provides a crucial pseudocapacitive contribution to supercapacitors. Thus, the flexible supercapacitor assembled with the PVA/CMCS-[ViEtIm][Br] hydrogel at a thickness of 0.1 mm has an areal specific capacitance of 314.4 mF cm^{-2} and an energy density of 78.6 μWh cm^{-2} at 540 μW cm^{-2}, with a capacitance retention of 87.5% after 10 000 charge/discharge cycles. Moreover, the flexible supercapacitor can also exhibit stable performance at different bending angles. This work provides a simple and feasible method for realizing ultra-thin flexible capacitors with high energy density.

1. Introduction

In recent decades, the critical situation faced in terms of energy shortages and the intermittent and unstable nature of renewable energy sources have fuelled the rapid development of energy storage devices.[1–3] As electronic devices are becoming thinner and more flexible, providing energy for these wearable electronic devices has become an urgent problem. In order to better address this problem, the development of high-performance electrochemical energy storage devices such as supercapacitors (SCs) has become particularly important. SCs are more suitable for high-power applications and long-cycling performance than batteries.[4] Since the energy density (E) of a solar cell has a positive relationship with the voltage (V) and the square of the specific capacitance (C), *i.e.*, $E = 1/2\ CV^2$, an increase in energy density can be achieved by improving these two parameters. Various methods have been explored to increase the energy density of energy storage devices such as the use of asymmetric capacitors or the development of pseudo-capacitive electrode materials.[5–7] For the development of high-performance SCs, various forms of carbon are used as electrodes, which have received much attention worldwide due to their high electronic conductivity, large surface area, layered porosity and chemical inertness with other components of SCs.[8–11] As a key component of energy storage devices, electrolytes have a significant impact on the overall device performance including voltage (V).[12] To improve the capacitance and energy density of SCs, the development of redox-active electrolytes emerges as another promising approach.[13–15] A number of redox-active substances have been reported to be introduced into electrolytes to generate redox reactions at the electrode/electrolyte contact interface to increase the energy density by increasing the pseudocapacitance, such as hydroquinone, potassium iodide and decamethylferrocene.[16–20] This approach increases the capacitance by introducing a redox substance or a mediator into the polymer, so that the redox substance or mediator is in the solid electrolyte, and the conductivity of the electrolyte is improved while providing an additional charge to store the capacitance through the Faraday reaction. Redox-activated hydrogel polymer electrolytes have a great advantage over

[a]*Key Laboratory of Eco-functional Polymer Materials of the Ministry of Education, Key Laboratory of Polymer Materials of Gansu Province, College of Chemistry and Chemical Engineering, Northwest Normal University, Lanzhou 730070, China. E-mail: magf@nwnu.edu.cn*
[b]*College of Chemistry and Chemical Engineering, Lanzhou City University, Lanzhou 730070, China*
[c]*School of Engineering, Westlake University, Hangzhou 310024, China. E-mail: xuyuxi@westlake.edu.cn*

†Electronic supplementary information (ESI) available. See DOI: https://doi.org/10.1039/d4lp00007b

‡These authors contributed equally to this work. They should thus be considered co-first authors.

other solid electrolytes by having a high ionic conductivity of 10^{-3} S cm^{-1}–10^{-2} S cm^{-1}, and the ionic conductivity of hydrogel polymer electrolytes is important for the realization of flexible supercapacitors. Meanwhile, another advantage of redox hydrogel polymer electrolytes can be realized by using redox substances or mediators to alleviate the ion depletion problem during charging.[21] In addition, the solid-state electrolyte acts as a moderate ionic conductor and a separator, greatly reducing the package size and cost. Among them, hydrogel electrolytes constructed by combining cross-linked polymer networks with aqueous solutions have the advantages of excellent ionic conductivity, low fire hazards and low cost.[22] Therefore, in order to further adapt flexible supercapacitors (FSCs) to human needs, the development of redox-active polymer hydrogel electrolytes (PHEs) is of great significance.

PHEs are porous soft materials consisting of a cross-linked polymer network containing large amounts of water. Due to their high mechanical properties, flexibility, elasticity and biocompatibility, they have become widely promising electrolyte matrices for energy conversion and storage systems in recent years.[23–25] Zhang *et al.*[26] proposed the graft copolymerization of polyacrylic acid (PAAS) with carboxylated chitosan followed by strong uptake of KOH electrolyte to prepare an alkali-tolerant hydrogel electrolyte membrane with high ionic conductivity and pH responsiveness. Abbas Ali Hor *et al.*[27] proposed a membrane consisting of ~80 wt% ionic liquid (BMPTFSI) and redox additive ionic liquid (BMPBr) wrapped in an ~20 wt% polymer (PVDF–HFP) matrix as a flexible and self-contained thin film PHE for SCs. The application of natural polysaccharides in the field of hydrogels has attracted wide interest from researchers due to their abundant reserves, biocompatibility, non-toxicity, renewability, degradability, and cost-saving advantages.[28–30] Among the materials reported so far for PHEs, water-soluble PVA is the most widely studied and contains a large amount of –OH. Furthermore, carboxymethyl chitosan is a common natural polysaccharide material with good film-forming properties due to its rich hydrophilic groups and can be functionalized by appropriate modifications.[31] 1-Vinyl-3-ethylimidazolium bromide salt ([ViEtIm][Br]) is a common redox-active substance with a wide electrochemical window (generally above 3.5 V) and high electrochemical stability, which is characteristic of ionic liquids.[21]

Herein, we prepared a novel ionic liquid-filled poly(vinyl alcohol)/carboxymethyl chitosan-1-vinyl-3-ethylimidazolium bromide salt (PVA/CMCS-[ViEtIm][Br]) ultrathin hydrogel electrolyte film by a coating and freezing/thawing method, which is redox-active and stretchable, and assembled into a flexible supercapacitor with very good electrochemical performance and potential for practical applications. Among them, polyvinyl alcohol (PVA) is a polymer matrix, carboxymethyl chitosan (CMCS) is a natural polymer additive, and 1-vinyl-3-ethylimidazolium bromide salt ([ViEtIm][Br]) is a redox active substance for flexible ultra-thin supercapacitors. The effects of hydrogel electrolyte films with different CMCS contents, thicknesses and [ViEtIm][Br] concentrations on their electrochemical properties were investigated in detail.

2. Experimental section

2.1. Preparation of the PVA/CMCS-[ViEtIm][Br] hydrogel

2 g of PVA and 0.2 g of CMCS were dissolved in 20 mL of deionized water at 90 °C and stirred for 2 h to obtain a uniform and transparent mixed solution. Then, the transparent solution was transferred to the coating machine to prepare the composite film with a thickness of 0.10 mm. Subsequently, the composite film was prepared as a cross-linked hydrogel film by freeze-thawing at −20 °C and room temperature alternately for 12 hours. Finally, the hydrogel film was immersed in a 1 M H_2SO_4 solution containing 3 wt% [ViEtIm][Br] at room temperature and kept for 6 hours to obtain a double mesh PVA/CMCS-[ViEtIm][Br] hydrogel.

For comparison, PVA/CMCS hydrogel films with different CMCS contents (0, 0.1, 0.2 and 0.3 g) were prepared by the same above-mentioned method. In addition, the PVA/CMCS-[ViEtIm][Br] hydrogel films immersed in 1 M H_2SO_4 solution with different concentrations of [ViEtIm][Br] (0, 1 wt%, 3 wt% and 5 wt%) were also investigated.

3. Results and discussion

Fig. 1 shows a schematic diagram of the preparation process of the PVA/CMCS-[ViEtIm][Br] hydrogel film constructed by physical crosslinking of binary polymer interpenetrating networks. In this process, the first network of CMCS is formed by ionic bonding between NH_3^+ and COO– and hydrogen bonding between –COOH and $–NHCOCH_3$ through non-covalent interactions; on the other hand, PVA and CMCS can be physically cross-linked through hydrogen bonds to form an interpenetrating network structure (second network) during freeze–thaw cycling. Thus, the PVA/CMCS hydrogel has a high electrolyte adsorption capacity due to the presence of hydrophilic groups such as $–NH_2$, –OH, –COOH and –NHCO–.[32] Finally, [ViEtIm][Br] was introduced into the PVA/CMCS hydrogel network as a redox active substance, which can additionally contribute to faradaic pseudocapacitance at the electrode/elec-

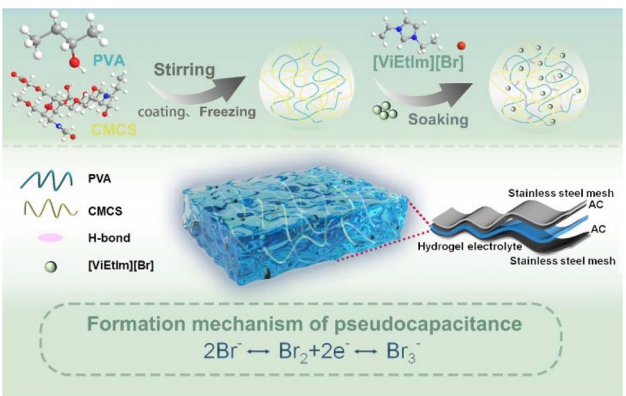

Fig. 1 Schematic diagram of the synthesis of the PVA/CMCS-[ViEtIm][Br] hydrogel electrolyte.

trolyte interface based on carbon-based electrochemical energy storage.

The thickness of the hydrogel film is measured using a thickness gauge. The PVA/CMCS-[ViEtIm][Br] hydrogel presented a homogeneous and smooth film with a thickness of 0.10 mm (Fig. 2a), which is shown in the inset. The transparent and smooth state of the gel can also be seen in Fig. S1.† The surface structure of the hydrogel was characterized using SEM. Fig. S2† shows the SEM image of the PVA hydrogel, which shows that the PVA hydrogel contains a porous structure. Fig. 2b and c show the freeze-dried PVA/CMCS and PVA/CMCS-[ViEtIm][Br] PHEs. It can be seen that the surface of the freeze-dried PVA/CMCS gel shows a large number of folds, while the surface of the freeze-dried PVA/CMCS-[ViEtIm][Br] gel shows a porous structure. Such a porous structure can facilitate the transport of ions and thus improve correlation kinetics. Fig. 2d shows the XRD patterns of PVA, CMCS and PVA/CMCS-[ViEtIm][Br] after freeze-drying. It can be observed that CMCS exhibits a weaker crystal peak at 2θ = 20.4°, indicating a typical polymer amorphous structure. PVA is a semi-crystalline polymer, which shows that an obvious crystalline peak exists at 2θ = 20°. When PVA was cross-linked with CMCS to form an interpenetrating network structure, the intensity of the peak near 2θ = 20° significantly reduced, indicating that the cross-linked copolymer became a disordered amorphous structure with low crystallinity.[23] Apparently, the regularity of the original PVA is destroyed by cross-linking, which leads to the formation of amorphous copolymers. Fig. 2e shows the FT-IR plots of PVA, PVA/CMCS and PVA/CMCS-[ViEtIm][Br] after freeze-drying. In the PVA/CMCS-[ViEtIm][Br] hydrogel films, the peak at 1738.6 cm^{-1} corresponds to the stretching vibration of C=O in –COOH and the peak at 1644.5 cm^{-1} corresponds to the stretching vibration of C=O in $-NHCOCH_3$. Comparison with the characteristic peaks of PVA/CMCS shows that the CMCS chains provide –COOH and $-NHCOCH_3$, between which hydrogen bonds can be formed. The peak at 1069.6 cm^{-1} is attributed to C=O and C–O–C. The peaks at 1616.5 and 1443.6 cm^{-1} are attributed to the tensile vibrations of C–O in $-COO^-$ on the CMCS chains, and it can form an ionic bond with the positively charged NH_3^+ in the CMCS chain. The peaks at 3432.2 cm^{-1} and 2914.4 cm^{-1} are attributed to the stretching vibrations of –OH and C–H in PVA.[31,32] It can be noticed that the introduction of the CMCS molecular chain, which increases the –OH content, leads to broadening of the peaks at around 3430.1 cm^{-1} for the PVA/CMCS and PVA/CMCS-[ViEtIm][Br] curves as compared to the curve for pure PVA.[28] The above information indicates the successful preparation of the PVA/CMCS-[ViEtIm][Br] PHE film.

In order to test the mechanical properties of the prepared PVA/CMCS-[ViEtIm][Br] hydrogel film, bending, twisting, and stretching tests are performed. As shown in Fig. 2f, the elongation at break of the PVA hydrogel film is 493%. With the introduction of CMCS, the elongation at break of the PVA/CMCS hydrogel film increased to 615%. The introduction of [ViEtIm][Br] further increased the elongation at break of the PVA/CMCS-[ViEtIm][Br] hydrogel film to 785%. The variation of hydrogel tensile properties with the concentrations of CMCS, thickness and [ViEtIm][Br] content is shown in Fig. S3, S4 and S5.† As the thickness of the gel film gradually increases, the elongation at break of the gel becomes larger and reaches a maximum of 615% at a thickness of 0.1 mm. This may be due to the increase in PVA and CMCS content that accompanies the increase in gel thickness, the intertwining of the CMCS molecular chains with the PVA polymer chains, and the enhanced hydrogen-bonding cross-linking between the molecular chains, which improves the elongation at break of the hydrogel films. With the increase in [ViEtIm][Br] content, the hydrogen bonding and electrostatic interactions within the gel film are enhanced, which improves the elongation at break of the hydrogel film. As shown in Fig. 2g–i, the prepared PVA/CMCS-[ViEtIm][Br] hydrogel film shows no cracks or breaks after bending and twisting, exhibiting good flexibility and mechanical properties.

The FSCs are first assembled using commercial activated carbon (AC) as the electrode material and PVA/CMCS hydrogel films with different CMCS contents (0, 0.1, 0.2 and 0.3 g) as PHEs. Fig. 3a shows the comparative CV curves of PVA/CMCS hydrogel-based FSCs containing different CMCS contents at 50 mV s^{-1}. The CV curve area increases as the CMCS content increases, and when the CMCS content exceeds 0.2 g, the CV curve area decreases because the excess CMCS is not favorable for ion transport in PHEs. The increase in CMCS makes the 3D network voids smaller, making it difficult for water molecules and solvated electrolyte ions to enter the hydrogel network, which increases the transport resistance of electrolyte ions.[32] Obviously, the area of the CV curve is the largest when the

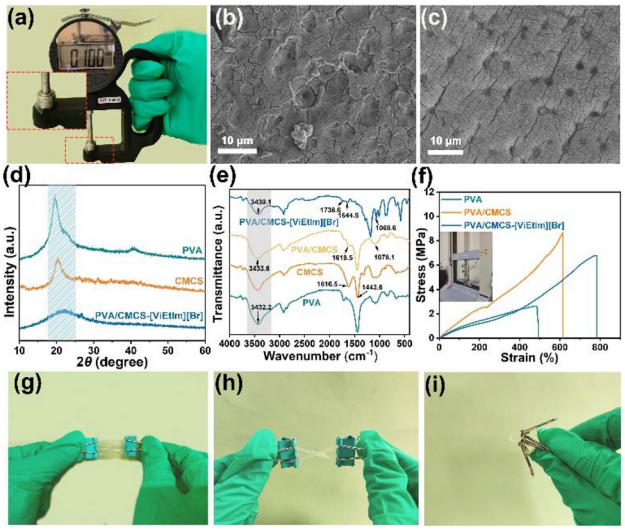

Fig. 2 (a) The thickness test of the PVA/CMCS-[ViEtIm][Br] hydrogel (the inset is the photo of the tested hydrogel), SEM images of (b) PVA/CMCS gel and (c) PVA/CMCS-[ViEtIm][Br] gel, (d) XRD patterns and (e) FT-IR images of PVA, CMCS, PVA/CMCS and PVA/CMCS-[ViEtIm][Br], (f) the stress–strain curves of PVA, PVA/CMCS and PVA/CMCS-[ViEtIm][Br] hydrogels, and (g–i) twisting and bending of the PVA/CMCS-[ViEtIm][Br] hydrogel.

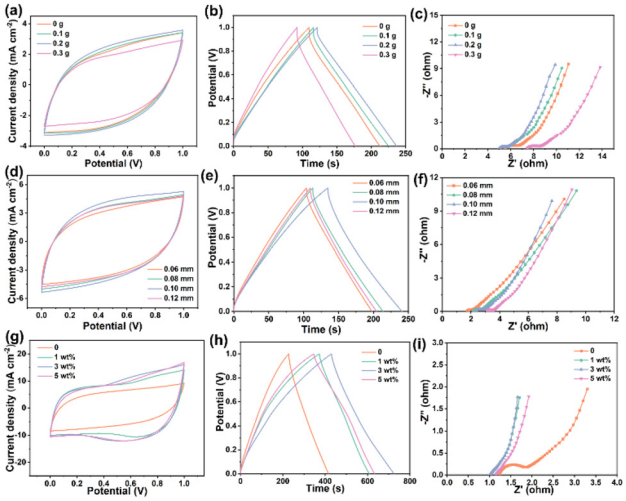

Fig. 3 Electrochemical performance of PVA/CMCS hydrogel-based FSCs with different contents of CMCS: (a) comparison of CV curves, (b) GCD curves, and (c) Nyquist curves. Electrochemical performance of PVA/CMCS hydrogel-based FSCs with different thicknesses: (d) comparison of CV curves, (e) GCD curves, and (f) Nyquist curves. Electrochemical performance of PVA/CMCS-[ViEtIm][Br] hydrogel-based FSCs with different concentrations of [ViEtIm][Br]: (g) comparison of CV curves, (h) GCD curves, and (i) Nyquist curves.

CMCS content is 0.2 g, indicating that it has the most excellent capacitance behavior. Fig. S6† shows the electrochemical properties of the hydrogel at different scan rates at a CMCS content of 0.2 g, showing good electrochemical properties. For the GCD curves in Fig. 3b, the same variation trend as in CV curves is evident. The optimal areal specific capacitance of the PVA/CMCS hydrogel-based FSC with a CMCS content of 0.2 g is 121.4 mF cm^{-2} at an operating voltage range of 0 to 1 V and a current density of 0.5 mA cm^{-2}. The GCD curves at different current densities at a CMCS content of 0.2 g in Fig. S7† can also illustrate that the hydrogel has a favorable charge/discharge behavior. Meanwhile, PVA/CMCS with a CMCS content of 0.2 g shows significantly lower interfacial resistance and charge transfer resistance than other FSCs in the comparative Nyquist curve plot (Fig. 3c). Thus, PVA/CMCS with a CMCS content of 0.2 g was used as the optimal sample.

As is known, the thickness of the hydrogel electrolyte film directly affects the ion transport inside the PHEs. Fig. 3d shows the comparative CV curves of PVA/CMCS hydrogel-based FSCs with different thicknesses at 50 mV s^{-1}. The CV curves of PVA/CMCS hydrogel-based FSCs with different thicknesses all show a rectangular-like shape, indicating an electrochemical double layer capacitance (EDLC) behavior. The CV curve area is largest when the thickness of the PVA/CMCS hydrogel film is 0.10 mm, indicating that it has the largest areal specific capacitance. Fig. 3e shows the GCD curves of PVA/CMCS hydrogel-based FSCs with different thicknesses at a current density of 0.5 mA cm^{-2} with an operating voltage of 0–1.0 V. The PVA/CMCS hydrogel film with a thickness of 0.10 mm presents the longest discharge time and shows a high areal specific capacitance of 127.6 mF cm^{-2} at 0.5 mA cm^{-2}. Meanwhile, Fig. 3f shows the comparison of the Nyquist curves of PVA/CMCS hydrogel-based FSCs with different film thicknesses. It can be seen that the interfacial resistance (R_s) and charge transfer resistance (R_{ct}) of FSCs gradually increase with increasing thickness, which is due to the fact that ion transport becomes more difficult with increasing thickness. By comprehensive comparison, the thickness of the PVA/CMCS hydrogel film of 0.10 mm is selected as the optimal thickness.

To investigate the effect of [ViEtIm][Br] on the electrochemical properties of FSCs, CV tests are performed for PVA/CMCS-[ViEtIm][Br] hydrogel-based FSCs with different [ViEtIm][Br] concentrations at 50 mV s^{-1}. As shown in Fig. 3g, the CV curves of PVA/CMCS hydrogel-based FSCs show obvious rectangular-like shapes, which is due to the EDLC energy storage mechanism in carbon-based SCs. However, PVA/CMCS-[ViEtIm][Br] hydrogel-based FSCs exhibit obvious redox peaks after the introduction of [ViEtIm][Br], which is due to the occurrence of a redox reaction and the generation of pseudocapacitance. The reaction mechanism for the formation of pseudocapacitance is as follows:[33]

$$2Br^- \leftrightarrow Br_2 + 2e^- \leftrightarrow Br_3^- \quad (1)$$

As shown in Fig. 3g, the integrated area of PVA/CMCS-[ViEtIm][Br] hydrogel-based FSCs with the [ViEtIm][Br] concentration of 3 wt% is larger than that of PVA/CMCS and other concentrations of PVA/CMCS-[ViEtIm][Br] hydrogel-based FSCs, indicating that the former possesses a higher specific capacitance. The redox reaction resulting from the introduction of [ViEtIm][Br] provides a stable pseudocapacitance for flexible hydrogel electrolyte devices to extend the specific capacitance and energy density.[34] As shown in Fig. 3h, the GCD curves of PVA/CMCS-[ViEtIm][Br] hydrogel-based FSCs with [ViEtIm][Br] also demonstrate the interfacial redox activity contribution. The PVA/CMCS-[ViEtIm][Br] hydrogel-based FSCs show the longest discharge time when the [ViEtIm][Br] concentration is 3 wt%, which indicates a higher areal specific capacitance than others. Fig. 3i shows the Nyquist curves of PVA/CMCS-[ViEtIm][Br] hydrogel-based FSCs with different [ViEtIm][Br] concentrations. It can be clearly seen that the introduction of [ViEtIm][Br] can increase the ionic conductivity of PVA/CMCS-[ViEtIm][Br] hydrogel-based FSCs, allowing ions to quickly transfer/diffuse to the electrode surface, thereby improving the electrochemical performance of FSCs. The smallest R_s and R_{ct} of PVA/CMCS-[ViEtIm][Br] hydrogel-based FSCs exist when the [ViEtIm][Br] concentration is 3 wt%. The R_s and R_{ct} values of PVA/CMCS-[ViEtIm][Br] hydrogel-based FSCs increased when the [ViEtIm][Br] concentration was 5 wt%. This may be due to the increase in [ViEtIm][Br] content, which increases the viscosity of the electrolyte to a certain extent, leading to a decrease in ionic conductivity.[35] Therefore, the [ViEtIm][Br] concentration of 3 wt% is selected as the optimal amount to be added to the PVA/CMCS-[ViEtIm][Br] hydrogels for subsequent electrochemical performance studies.

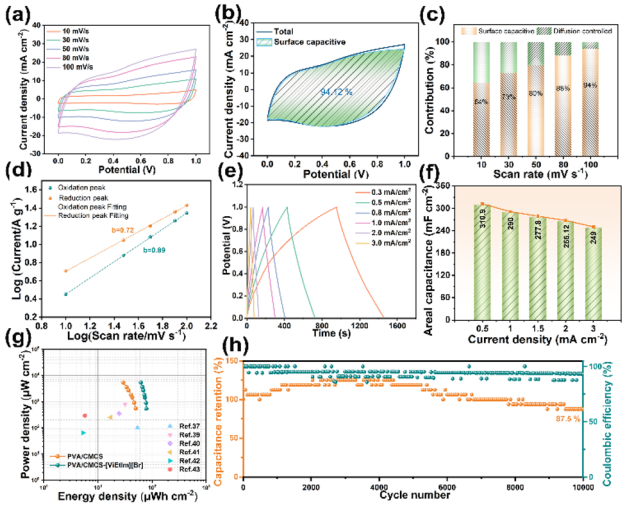

Fig. 4 (a) CV curves of the PVA/CMCS-[ViEtIm][Br] hydrogel-based FSC, (b) surface capacitive contribution, (c) ratio of surface and diffusion control to capacitance contribution, (d) log(current) *vs.* log(scan rate) plot, (e) GCD curve of the PVA/CMCS-[ViEtIm][Br] hydrogel-based FSC, (f) area capacitance curves, (g) Ragone diagram of PVA/CMCS and PVA/CMCS-[ViEtIm][Br] hydrogel-based FSCs and its comparison with previously reported works, and (h) cycling stability of the PVA/CMCS-[ViEtIm][Br] hydrogel-based FSC.

Fig. 4a shows the CV curves of PVA/CMCS-[ViEtIm][Br] hydrogel-based FSCs at different scan rates from 10 to 100 mV s^{-1} with operating voltages from 0 to 1.0 V. It can be seen that the CV curves have similar shapes at different scan rates. The presence of distinct redox peaks in the PVA/CMCS-[ViEtIm][Br]hydrogel-based FSCs demonstrates that a reversible redox reaction occurred. Also, as the scan rate increases, their oxidation peaks are shifted in the positive direction and the reduction peaks are shifted in the negative direction, which is due to the mixed polarization of ion and electron resistance.[31,36] As shown in Fig. 4b, the surface capacitive contribution of PVA/CMCS-[ViEtIm][Br]-hydrogel-based FSCs reaches 94.12% at a scan rate of 100 mV s^{-1}, which is attributed to the occurrence of redox reactions and the generation of pseudocapacitance due to the introduction of [ViEtIm][Br]. The increase of the pseudocapacitance contribution can effectively improve the capacitance capability of supercapacitors. As follows from Fig. 4c, the contribution of the surface limiting capacitance is slightly higher than the diffusion controlled capacitance at low scan rates. As expected, the contribution of the surface capacitance increases with increasing scan rate from 64% to 94% when increasing from 10 mV s^{-1} to 100 mV s^{-1}, due to the lower kinetic confinement of the electrode surface at high scan rates. The *b*-value is determined as the slope of the log(i) *versus* log(ν) plot, as shown in Fig. 4d. To estimate the capacitance effect, the type of charge storage was analyzed at different scan rates using the following equation:

$$i(V) = a\nu^{b} \quad (2)$$

where a and b are adjustable parameters. The *b*-value is an important parameter from which information about the charge storage mechanism can be obtained. Values of b close to 1 and equal to 0.5 indicate that charge storage processes are dominated by surface-controlled redox reactions and absorption/desorption of electrolyte ions, while the latter indicates that diffusion-controlled Faraday processes dominate charge storage processes. The oxidation peak *b*-value of the carbon-based electrode in the PVA/CMCS-[ViEtIm][Br] hydrogel was 0.89 and the reduction peak *b*-value was 0.72, suggesting that the charge storage benefits from diffusion-controlled redox processes in the main body of the electrode material, as well as the formation of the bilayer and the surface Faraday reaction.[37,38]

Fig. 4e shows the GCD curves of PVA/CMCS-[ViEtIm][Br] hydrogel-based FSCs in the current density range of 0.3–3 mA cm^{-2} to study the rate performance of FSCs. The GCD curves for PVA/CMCS-[ViEtIm][Br] hydrogel-based FSCs are no longer typically linear due to the presence of [ViEtIm][Br] redox additives, but the charge/discharge times remain relatively symmetric for all current densities, indicating good and reversible electrochemical properties. Equations are applied to calculate the energy density (EA, μWh cm^{-2}) and power density (PA, μW cm^{-2}) based on the data in Fig. 4e. Fig. 4f shows the areal specific capacitance of PVA/CMCS-[ViEtIm][Br] hydrogel-based FSCs at different current densities. It can be clearly seen that the FSCs have high areal specific capacitances of 310.9 mF cm^{-2}, 290.1 mF cm^{-2}, 277.8 mF cm^{-2}, 266.12 mF cm^{-2} and 249.2 mF cm^{-2} at 0.5, 1.0, 1.5, 2.0 and 3.0 mA cm^{-2}, respectively. The corresponding volume specific capacities are 10.4 F cm^{-3}, 9.7 F cm^{-3}, 9.3 F cm^{-3}, 8.9 F cm^{-3}, and 8.3 F cm^{-3}. It is shown that PVA/CMCS-[ViEtIm][Br] hydrogel-based FSCs with 3 wt% [ViEtIm][Br] content exhibit outstanding rate performance, the value of which is better than that of PVA/CMCS [ViEtIm][Br] hydrogel-based FSCs with 0, 1 wt%, and 5 wt% [ViEtIm][Br] content (Fig. S8†). The specific capacitance decreases as the current density increases in a gradient, which is due to the effect of ion diffusion at different current densities.

Fig. 4g shows the Ragone diagram of PVA/CMCS and PVA/CMCS-[ViEtIm][Br] hydrogel-based FSCs. At a power density of 540 μW cm^{-2}, the energy density of the PVA/CMCS-[ViEtIm][Br] hydrogel-based FSC reaches a maximum of 78.6 μWh cm^{-2}, which is much better than the energy density of 50.25 μW cm^{-2} of the PVA/CMCS hydrogel-based FSC. These values are greater than the other previously reported FSCs shown in Table S1,† such as the FSC based on the poly(pyrrole-*co*-aniline) incorporated PVA/PEG gel electrolyte (54 μWh cm^{-2}),[37] the FSC with a self-healing PVA/phytic acid hydrogel electrolyte (31.7 μWh cm^{-2}),[39] and so on.[40–43] In addition, the cycling stability of the PVA/CMCS-[ViEtIm][Br] hydrogel-based FSCs is evaluated by subjecting them to 10 000 charge–discharge cycles at 1 mA cm^{-2}, and the result is shown in Fig. 4h. It can be seen that the PVA/CMCS-[ViEtIm][Br] hydrogel-based FSC has excellent cycling stability, retaining 87.5% of the initial capacitance after 10 000 cycles, and exhibits a high initial coulombic efficiency of 93.3% with virtually no losses.

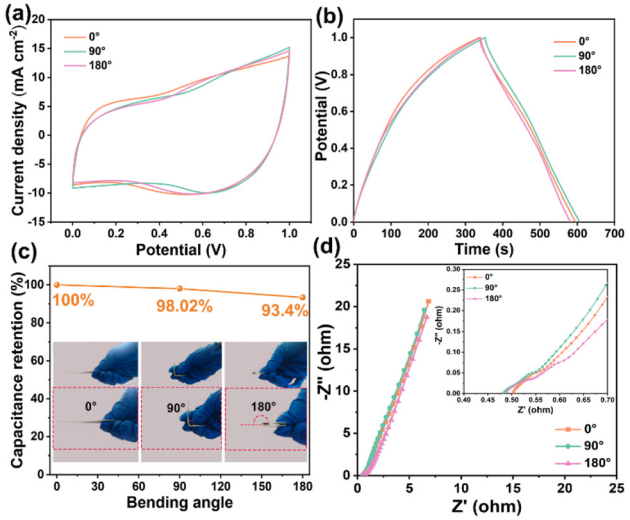

Fig. 5 PVA/CMCS-[ViEtIm][Br] hydrogel-based supercapacitors at different bending angles (0°, 90° and 180°): (a) CV curve, (b) GCD curve, (c) capacitance retention, and (d) Nyquist curve.

The electrochemical properties of the PVA/CMCS-[ViEtIm][Br] hydrogel-based FSCs are evaluated at different bending angles for practical applications. Fig. 5a shows the CV curves of PVA/CMCS-[ViEtIm][Br] hydrogel-based FSCs bent at 0°, 90° and 180° at 50 mV s^{-1}. The CV curves have a similar shape, indicating that the structure of FSCs remains intact even when bent at 180°. Fig. 5b shows the GCD curves of PVA/CMCS-[ViEtIm][Br] hydrogel-based FSCs bent at 0°, 90° and 180° at a current density of 0.5 mA cm^{-2}. It can be seen that the curves have a high degree of overlap at different bending angles, and the discharge time of PVA/CMCS-[ViEtIm][Br] hydrogel-based FSCs did not vary greatly. As shown in Fig. 5c, the PVA/CMCS-[ViEtIm][Br] hydrogel-based FSCs retain 93.4% of the initial capacitance at 180°, which indicates that the PVA/CMCS-[ViEtIm][Br]hydrogel-based FSCs have good power output at different bending angles. Fig. 5d shows the Nyquist curves of PVA/CMCS-[ViEtIm][Br]hydrogel-based FSCs at different bending angles of 0°, 90° and 180°, which indicates that they have good ionic conductivity at different bending angles. In conclusion, PVA/CMCS-[ViEtIm][Br] hydrogel-based FSCs have excellent flexibility, can adapt to bending at multiple angles and exhibit good electrochemical properties for practical applications.

4. Conclusions

In conclusion, a novel stretchable, ultrathin polyvinyl alcohol/carboxymethyl chitosan incorporated with 1-vinyl-3-ethylimidazolium bromide (PVA/CMCS-[ViEtIm][Br]) PHEs with redox activity was prepared by a facile coating and freezing/thawing method, which is further used as an electrolyte and separator to assemble ultra-thin FSCs. The PVA/CMCS-[ViEtIm][Br] PHEs exhibit good flexibility to stretch, bend and twist. More importantly, the redox reaction caused by the addition of [ViEtIm][Br] as a redox agent in the PHEs provides an important pseudocapacitive contribution to SCs, where Br^- is converted to Br_2 during charging and Br_2 is converted to Br_3^- during discharging. In addition, the energy density of PVA/CMCS-[ViEtIm][Br] hydrogel-based FSCs is greatly increased without sacrificing the power density. Specifically, the PVA/CMCS-[ViEtIm][Br]hydrogel-based FSCs exhibited a high area-ratio capacitance of 310.9 mF cm^{-2} at 0.5 mA cm^{-2}, achieved an excellent energy density of 78.6 μWh cm^{-2} at 540 μW cm^{-2} power density, and demonstrated good cycling stability with a capacitance retention of 87.5% after 10 000 cycles. The electrochemical performance of PVA/CMCS-[ViEtIm][Br] hydrogel-based FSCs is much higher than that of the PVA/CMCS hydrogel-based FSCs and the other previously reported FSCs. Moreover, the PVA/CMCS-[ViEtIm][Br] hydrogel-based FSCs can also exhibit stable performance at different bending angles, confirming their potential for practical applications. The proposed strategy of introducing redox active substances into flexible hydrogel electrolytes can not only increase the pseudocapacitance of supercapacitors, but also provide ideas for realizing high-performance flexible supercapacitors.

Author contributions

Mengmeng Xun: writing – original draft, methodology, software, formal analysis, and writing – review & editing; Xiuting Shi: methodology, formal analysis, investigation, and writing – original draft; Haiping Wang: methodology, software, formal analysis, investigation, and writing – original draft; Xiaoyan Li: validation and investigation; Wenxing Miao: investigation and formal analysis; Xiangbing Wang: investigation and methodology; Kanjun Sun: methodology and formal analysis; Hui Peng: conceptualization, resources, and funding acquisition; Guofu Ma: resources, funding acquisition, and supervision; Yuxi Xu: resources, methodology, writing revisions and supervision.

Conflicts of interest

The authors declare that they have no known competing financial interests or personal relationships that could have appeared to influence the work reported in this paper.

Acknowledgements

This study was supported by the National Natural Science Foundation of China (42167068 and 22269020), the Key Talent Project of Gansu Province in 2022 (2022RCXM078), and the Gansu Province Higher Education Industry Support Plan Project (2021CYZC-09 and 2023CYZC-68).

References

1 J. Bai, S. Hu, L. Feng, X. Jin, D. Wang, K. Zhang and X. Guo, *Chin. Chem. Lett.*, 2023, **109326**, 1001–8417.
2 M. R. Benzigar, V. D. B. C. Dasireddy, X. Guan, T. Wu and G. Liu, *Adv. Funct. Mater.*, 2020, **30**, 2002993.

3 Y. Wang, X. Wu, Y. Han and T. Li, *J. Energy Storage*, 2021, **42**, 103053.
4 Z. Yan, S. Luo, Q. Li, Z.-S. Wu and S. F. Liu, *Adv. Sci.*, 2023, 2302172.
5 H. W. Park and K. C. Roh, *J. Power Sources*, 2023, **557**, 232558.
6 S. Sahoo, R. P. Kumar, E. Joanni, R. K. Singh and J. Shim, *J. Mater. Chem. A*, 2022, **10**, 13190–13240.
7 C. Choi, D. S. Ashby, D. M. Butts, R. H. DeBlock, Q. Wei, J. Lau and B. Dunn, *Nat. Rev. Mater.*, 2020, **5**, 5–19.
8 L. Wang, X. Yao, D. Chen, J. Wang, Z. Zhang, J. Liu, T. Lin, W. Wang, Z. Hong, F. Huang and W. Wang, *Sci. China Mater.*, 2022, **65**, 391–399.
9 J. Liang, S. Luo, D. Pan, P. Xu, F. Zhan and J. Li, *Chem. Eng. J.*, 2023, **464**, 142646.
10 I. Pathak, B. Dahal, D. Acharya, K. Chhetri, A. Muthurasu, Y. R. Rosyara, T. Kim, S. Saidin, T. H. Ko and H. Y. Kim, *Chem. Eng. J.*, 2023, **475**, 146351.
11 M. Wang, J. Yang, S. Liu, X. Che, S. He, G. Chen and J. Qiu, *Chem. Eng. J.*, 2023, **451**, 138501.
12 Q. Zhang, L. Zhao and F. Ran, *Renewable Energy*, 2022, **194**, 80–88.
13 Z. Zhao, J. Lai, D. T. Ho, Y. Lei, J. Yin, L. Chen, U. Schwingenschlögl and H. N. Alshareef, *ACS Energy Lett.*, 2023, **8**, 608–618.
14 L. Sun, K. Zhuo, Y. Chen, Q. Du, S. Zhang and J. Wang, *Adv. Funct. Mater.*, 2022, **32**, 2203611.
15 W. Qin, N. Zhou, C. Wu, M. Xie, H. Sun, Y. Guo and L. Pan, *ACS Omega*, 2020, **5**, 3801–3808.
16 W. Yang, Q. Han, W. Li, M. Wu, J. Yao, M. Zhao and X. Lu, *Chem. Eng. J.*, 2022, **448**, 137731.
17 Y. Zhang, Y. Li, X. Wang, X. Teng, L. Guan, H. Yang, Z. He, Y. Wan, S. Guo, H. Hu and M. Wu, *J. Mater. Chem. A*, 2022, **10**, 19852–19858.
18 C. Strietzel, M. Sterby, H. Huang, M. Strømme, R. Emanuelsson and M. Sjödin, *Angew. Chem., Int. Ed.*, 2020, **59**, 9631.
19 H.-S. Fan, X. Liang, F.-X. Ma, G. Zhang, Z.-Q. Liu, L. Zhen, X. C. Zeng and C.-Y. Xu, *Small*, 2023, 2307863.
20 S. Giri and I. Dash, *J. Mater. Chem. A*, 2023, **11**, 16458–16493.
21 L. Zhang, S. Yang, J. Chang, D. Zhao, J. Wang, C. Yang and B. Cao, *Front. Chem.*, 2020, **8**, 413.
22 R. Zhao, Y. Wu, Z. Liang, L. Gao, W. Xia, Y. Zhao and R. Zou, *Energy Environ. Sci.*, 2020, **13**, 2386–2403.
23 R. Kumar and A. Parashar, *Wiley Interdiscip. Rev.: Comput. Mol. Sci.*, 2023, **13**, e1655.
24 X. Xu, V. V. Jerca and R. Hoogenboom, *Mater. Horiz.*, 2021, **8**, 1173–1188.
25 B. Wang, J. Li, C. Hou, Q. Zhang, Y. Li and H. Wang, *ACS Appl. Mater. Interfaces*, 2020, **12**, 46005–46014.
26 Q. Zhang, L. Zhao, H. Yang, L. Kong and F. Ran, *J. Membr. Sci.*, 2021, 0376–7388.
27 A. Hor, N. Yadav and S. Hashmi, *ACS Appl. Energy Mater.*, 2022, **5**, 7627–7641.
28 Q. Zhang, L. Zhao and F. Ran, *Renewable Energy*, 2022, 80–88.
29 S. Wang, Y. Wei, Y. Wang and Y. Cheng, *Carbohydr. Polym.*, 2023, **313**, 120760.
30 Q. Zheng, M. Shang, X. Li, L. Jiang, L. Chen, J. Long, A. Jiao, H. Ji, Z. Jin and C. Qiu, *Food Hydrocolloids*, 2024, **146**, 109190.
31 C. Zhao, X. Gong, L. Shen, Y. Wang and C. Zhang, *ACS Appl. Polym. Mater.*, 2022, **4**, 4025–4034.
32 M. Yu, X. Ji and F. Ran, *Carbohydr. Polym.*, 2021, **255**, 117346.
33 L. Fan, Q. Tu, C. Geng, J. Huang, Y. Gu, J. Lin, Y. Huang and J. Wu, *Electrochim. Acta*, 2020, **331**, 135425.
34 Y. Yang, D. Zhang, Y. Liu, L. Shen, T. Zhu, X. Xu, J. Zheng and X. Gong, *ACS Appl. Mater. Interfaces*, 2021, **13**, 34168–34177.
35 X. Ma, J. Yu, Y. Hu, J. Texter and F. Yan, *Ind. Chem. Mater.*, 2023, **1**, 39–59.
36 Y. Zhang, T. Zeng, W. Yan, D. Huang, Y. Zhang, Q. Wan and N. Yang, *Carbon*, 2022, **188**, 315–324.
37 L. Guo, W. Ma, Y. Wang, X. Song, J. Ma, X. Han, X. Tao, L. Guo, H. Fan, Z. Liu, Y. Zhu and X. Wei, *J. Alloys Compd.*, 2020, **843**, 155895.
38 J. Yang, B. Zhang, X. Tian, S. Liu, Z. Xu, G. Sun, G. Qin and Q. Chen, *J. Mater. Chem. C*, 2022, **10**, 17675–17683.
39 X. Gao, Q. Hu, K. Sun, H. Peng, X. Xie, H. A. Hamouda and G. Ma, *J. Alloys Compd.*, 2021, **888**, 161554.
40 C. Song, J. Yun, K. Keum, Y. Jeong, H. Park, H. Lee, G. Lee, S. Y. Oh and J. S. Ha, *Carbon*, 2019, 639–648.
41 K. Li, X. Liu, S. Chen, W. Pan and J. Zhang, *J. Energy Chem.*, 2019, **32**, 166–173.
42 G. K. Veerasubramani, K. Krishnamoorthy, P. Pazhamalai and S. J. Kim, *Carbon*, 2016, **105**, 638–648.
43 Z. Hou, H. Wang and K. Wang, *ChemNanoMat*, 2023, e202300422.